International Journal of Organizational Innovation

LOCALIZATIONS OF SOIL LIQUEFACTIONS INDUCED BY TECTONIC EARTHQUAKES

Tse-Shan Hsu
Department of Civil Engineering, Feng-Chia University
Taiwan R.O.C.
tshsu@fcu.edu.tw

Chang-Chi Tsao
Ph.D Program in Civil and Hydraulic Engineering, Feng-Chia University
Taiwan R.O.C.

Chihsen T. Lin
Department of Construction Engineering,
National Kaohsiung First University of Science and Technology
Taiwan R.O.C.

Abstract

There are four different types of earthquakes such as Tectonic, Volcanic, Collapse and Explosion. All these earthquakes will induce vibrations, yet only tectonic earthquakes will induce shear banding. Vibrations can be found everywhere in the earthquake disaster area, yet shear bandings can only be found in some localized areas. The images of soil liquefactions obtained in various countries in seismic zone have revealed that localizations of soil liquefactions only take place in tectonic earthquakes; for in-depth understanding of the cause of localizations of soil liquefactions, the authors of this article have developed the elasto-plastic strain softening material model and composed a finite element method program for simulation and analysis. The analysis result indicates that, even though comprehensive vibration in tectonic

earthquakes will induce excessive pore water pressure, the highly concentrated excessive pore water pressure existed in the shear band is the primary cause of localizations of soil liquefactions. Therefore, it is suggested that the conventional soil liquefaction potential evaluation method should be modified based on the cause of localizations of soil liquefactions in order to obtain the evaluation result consistent with actual situation.

Keywords: localization, soil liquefaction, tectonic earthquake, shear bandings.

Introduction

It has been revealed that the conventional cause of soil liquefaction is "With sufficiently high horizontal seismic coefficient k_h and sufficiently long earthquake duration while the ground water table is near ground surface, loose saturated sand strata within 20m of underground depth tend to compress and decrease in volume such that the induced excessive pore water pressure is greater than or equal to effective confining stress of soils thus inducing soil liquefaction."

Based on conventional cause, soil liquefactions can be divided into two different types: (1) the flow liquefaction which takes place when static shear stress is greater than liquefaction shear strength, where the major deformation is induced by static shear stress, and the cyclic shear stress only reduced shear strength of the soil; (2) the cyclic mobility takes place when the static shear stress is less than liquefaction shear strength, where the flowing deformation is induced by both static and cyclic shear stresses (Kramer, 1996).

Soil liquefaction will result in building damage during earthquake, thus design engineers must carry out evaluation of soil liquefaction potential as stipulated in Seismic Design Specifications and Commentary of Buildings (2006).

The conventional methods for evaluation of soil liquefaction potential include using simple criteria and simplified procedures. Simple criteria can be used for initial evaluation of liquefaction potential in large area; simplified procedures are empirical methods based on onsite test result, where the onsite tests include standard penetration test, cone penetration test, and shear wave velocity test. Currently the frequently used calculation analysis methods include Japan Road Associa-

tion Method (1996), Seed Method (1987; 1990), and Tokimatsu and Yoshimi Method (1983). Among them, Japan Road Association Method (1996) is the soil liquefaction potential evaluation method adopted by Seismic Design Specifications and Commentary of Buildings (2006).

For a certain position, when depth z falls within the range of 0~20m, the safety factor against liquefaction $F_L(z)$ is defined as the ratio of the computed cyclic resistance ratio (R_z) for the soil at this depth to cyclic stress ratio (L_z) generated by the design earthquake (Ishihara 1985; 1993; Seed 1987; Seed and Harder 1990); and then the liquefaction potential of this position P_L can be calculated by the equation proposed by Iwasaki, Tokida and Tatsuoka (1981) (as shown in Eq. 1).

$$P_L = \sum_{i=1}^{n} F_i(z) \cdot W_i(z) \cdot \Delta z_i \quad \ldots\ldots\ldots (1)$$

In the equation above, $F_i(z)$=1-$(F_L)_i$, $W_i(z)$=10-0.5 z_i, Δz_i is the thickness of the i^{th} layer counting from the ground surface. As for the calculated P_L, when P_L=0, there is no liquefaction potential; when $0<P_L \leqq 5$, there is minor liquefaction potential; when $5<P_L \leqq 15$, there is moderate liquefaction potential; when $15<P_L$, there is high liquefaction potential.

For different positions with identical horizontal seismic coefficient k_h, geological condition, and ground water table, the results of liquefaction potential evaluations will all be the same. Take Tainan City of Taiwan as an example, with k_h=0.33 and the ground water table close to ground surface, the soil liquefaction potential diagram published by Central Geological Survey, MOEA based on conventional soil liquefaction potential evaluation method is as shown in Figure 1; in Figure 1 the evaluation revealed that all areas covered by alluvial soil layer in Tainan City are equipped with high, moderate, or low soil liquefaction potential.

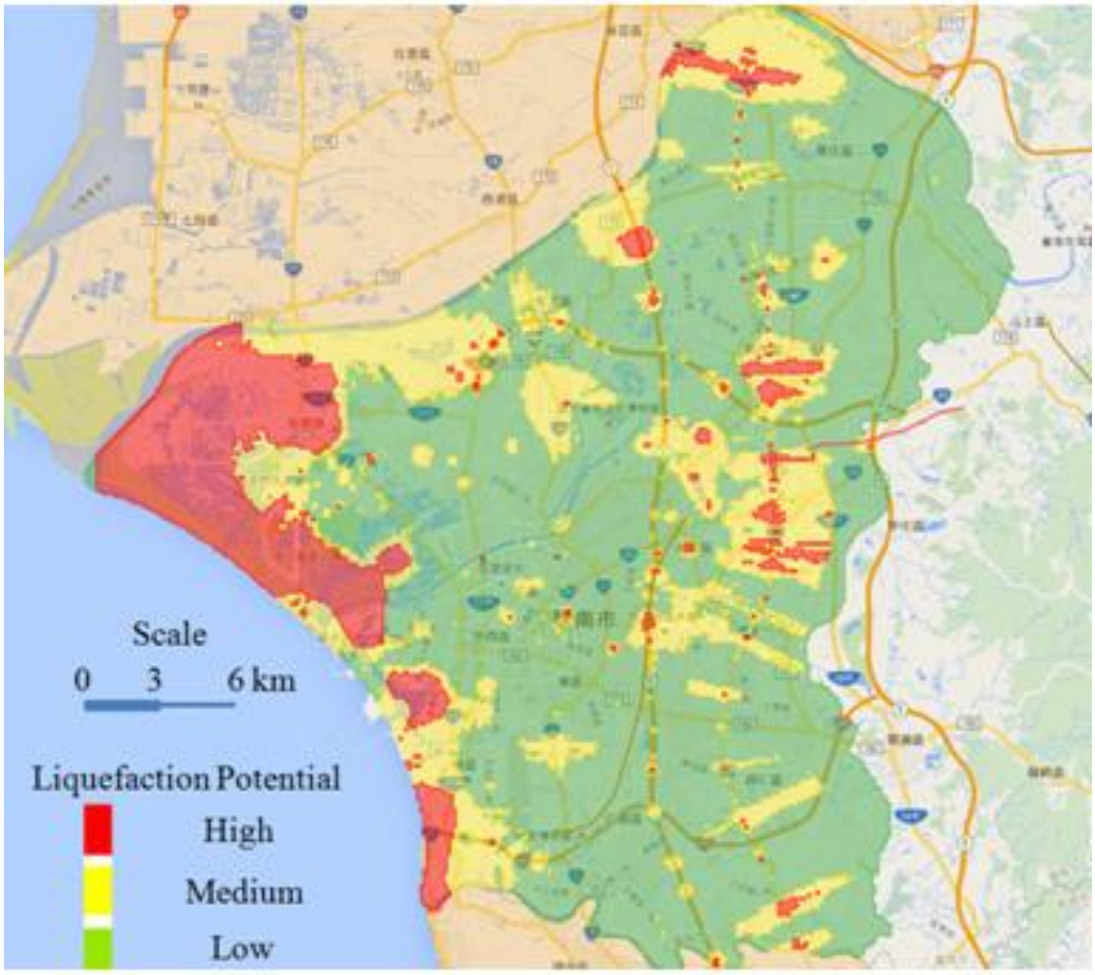

Figure 1. Distribution of soil liquefaction potentials in Tainan City of Taiwan (Central Geological Survey, MOEA, 2016)

The actual location of soil liquefaction in Tainan City took place during Meinong Earthquake on February 6th, 2016 is as shown in Figure 2; it has been revealed in Figure 2 that: (1) soil liquefaction was merely a kind of localized phenomenon; (2) the actual area of soil liquefaction is far less than the area of soil liquefaction potential announced by Central Geological Survey, MOEA; (3) the actual locations of soil liquefaction were mostly outside the areas with high liquefaction potentials. Thus we know that the conventional cause of soil liquefaction is different from the cause of localizations of soil liquefactions. The result of soil liquefaction potential evaluation obtained from conventional cause of soil liquefaction cannot fully reflect the actual localizations of soil liquefactions behavior.

To capture the localizations of soil liquefactions, it is known that localizations of deformations have to be produced during tectonic earthquakes during tectonic earthquakes before obtaining the highly concentrated excessive pore water pressure in the shear bands. Thus it is necessary to investigate the cause of localizations of soil liquefactions via simulation and analysis of tectonic earthquakes.

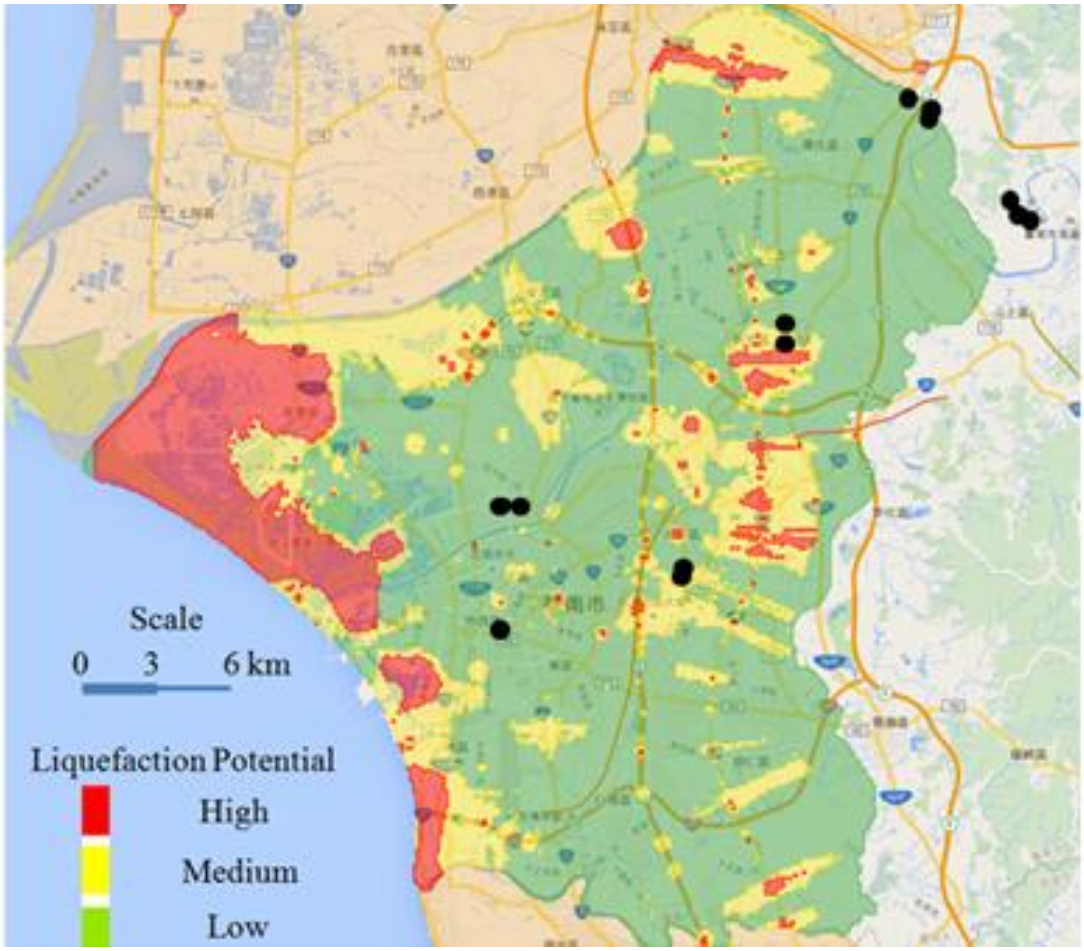

Figure 2. Comparison between the locations of soil liquefactions induced by Meinong Earthquake and the distribution of liquefaction potentials (Central Geological Survey, MOEA, 2016)

Formulation Of Constitutive Equation

Molenkamp (1985) expressed the physical meaning of the stiffness ratio, H/2G, as equal to the ratio of the elastic incremental deviatoric strain to the plastic incremental deviatoric strain if the partial derivatives of the yield sur-

face, F = 0, are normalized with $\partial F/\partial S_{ij}$ which is the partial derivative of the yield surface with respect to the deviator stress, S_{ij}. A quantity called octahedral shear strain (γ_{oct}) is frequently used in engineering practices. The stiffness ratio and the plastic octahedral shear strain, γ_{oct}^{p}, are closely related to each other because the deviatoric strain is proportional to the octahedral shear strain. Thus it makes more sense to use the stiffness ratio and the plastic octahedral shear strain to update the size of the yield surface. The proposed yield function, F, is then expressed as follows:

$$F = J_{2D}^{1/2} - \left(\kappa + H\,\gamma_{oct}^{P}\right) = 0 \quad \text{.....(2)}$$

where

J_{2D} = the second invariant of deviatoric stress;

κ = the size of the initial yield surface;

γ_{oct}^{p} = the plastic octahedral shear strain;

$H/2G$ = the strain softening parameter；

G = the shear modulus.

Differentiating Equation 1 leads to

$$dF = \frac{\partial F}{\partial \sigma'_{ij}}\sigma'_{ij} + \frac{\partial F}{\partial \gamma_{oct}^{p}} d\gamma_{oct}^{p} = \frac{\partial F}{\partial \sigma'_{ij}} d\sigma'_{ij} - H\, d\gamma_{oct}^{p} = 0 \quad \text{..... (3)}$$

where

$d\sigma'_{ij}$ = the incremental effective stress vector;

$d\gamma_{oct}^{p}$ = the incremental plastic octahedral shear strain;

The plastic incremental octahedral shear strain can be found as follows:

$$\left(d\gamma_{oct}^{p}\right)^2 = \frac{1}{9}\left[(d\varepsilon_{11}^{p} - d\varepsilon_{22}^{p})^2 + (d\varepsilon_{22}^{p} - d\varepsilon_{33}^{p})^2 + (d\varepsilon_{33}^{p} - d\varepsilon_{11}^{p})^2\right] + \frac{2}{3}\left[(d\varepsilon_{12}^{p})^2 + (d\varepsilon_{23}^{p})^2 + (d\varepsilon_{31}^{p})^2\right] \text{..... (4)}$$

The flow rule is:

$$d\varepsilon_{ij}^{p} = \lambda \frac{\partial F}{\partial \sigma'_{ij}} = \lambda \left(\frac{1}{2} J_{2D}^{-1/2} S'_{ij} \right) \ldots\ldots (5)$$

Substitution of Equation 5 into Equa- tion 4 leads to:

$$\begin{aligned} \left(d\gamma_{oct}^{p}\right)^2 &= \frac{1}{9}\left(\frac{\lambda}{2} J_{2D}^{-1/2} \right)^2 \left[(S_{11}-S_{22})^2 + (S_{22}-S_{33})^2 + (S_{33}-S_{11})^2 \right] \\ &\quad + \frac{2}{3}\left(\frac{\lambda}{2} J_{2D}^{-1/2} \right)^2 \left[(S_{12})^2 + (S_{23})^2 + (S_{31})^2 \right] \qquad \ldots\ldots (6) \\ &= \frac{\lambda^2}{6} \end{aligned}$$

Therefore

$$d\gamma_{oct}^{p} = \frac{\lambda}{\sqrt{6}} \ldots\ldots (7)$$

Substitution of Equation 7 into Equa- tion 3 leads to:

$$dF = \frac{\partial F}{\partial \sigma'_{ij}} d\sigma'_{ij} - \frac{1}{\sqrt{6}} H \lambda = 0 \ldots\ldots (8)$$

The incremental effective stress vector is

$$d\sigma'_{ij} = \overline{D}_{ijkl}^{e} \left(d\varepsilon_{kl} - d\varepsilon_{kl}^{p} \right) = \overline{D}_{ijkl}^{e} \left(d\varepsilon_{kl} - \lambda \frac{\partial F}{\partial \sigma'_{kl}} \right) \ldots\ldots (9)$$

Substituting Equation 9 into 8 leads to

$$\lambda = \frac{\frac{\partial F}{\partial \sigma'_{ij}} \overline{D}^{e}_{ijkl} d\underline{\varepsilon}}{\frac{1}{\sqrt{6}} H + \frac{\partial F}{\partial \sigma'_{ij}} \overline{D}^{e}_{ijkl} \frac{\partial F}{\partial \sigma'_{kl}}} \quad \ldots\ldots (10)$$

The stress-strain matrix is therefore can be obtained as follows:

$$\overline{D}^{ep}_{ijkl} = \overline{D}^{e}_{ijkl} - \overline{D}^{p}_{ijkl}$$

$$= \overline{D}^{e}_{ijkl} - \overline{D}^{e}_{ijkl} \frac{\partial F}{\partial \sigma'_{kl}} \frac{\partial F}{\partial \sigma'_{ij}} \overline{D}^{e}_{ijkl} \left[\frac{1}{\sqrt{6}} H + \frac{\partial F}{\partial \sigma'_{ij}} \overline{D}^{e}_{ijkl} \frac{\partial F}{\partial \sigma'_{kl}} \right]^{-1} \quad \ldots\ldots (10)$$

Using bulk modulus of water B_w and volumetric strain $\delta_{ij} d\varepsilon_{ij}$, the excess pore water pressure increment du_e is calculated as follows:

$$du_e = B_w \delta_{ij} \varepsilon_{ij} \quad \ldots\ldots (11)$$

where δ_{ij} is the Kronecker delta.

Numerical Analysis

For a 5.08cmx2.54cm plate shown in Figure 3 under plane strain conditions loaded at both ends, where the movement in the direction perpendicular to the loading is constrained, the uniform 50 x 25 mesh is used to analyze the behavior of the plate under uniformly prescribed loading conditions. Material properties used are: (1) the initial size of yield surface, κ, equal to 24kPa, (2) the Young's modulus, *E*, equal to 1200kPa, (3) Poisson's ratio, ν, equal to0.3, (4) the shear modulus, *G*, equal to 462kPa, (5) the bulk modulus of water, B_w, equal to 2140MPa, and (6) the strain softening parameter, *H*/2*G*, equal to -0.05 (for modeling strain softening behavior).

Results And Discussion

The behavior of localizations of deformations and the excessive pore water pressure contours under loading conditions are shown in Figures 4 and 5, respectively. Figure 4 shows when shear strains are deep into plastic range, shear bandings induced by localizations of deformations are captured due to the loss of symmetry and ellipticity. Figure 5 indicates that the distribution of the excess pore water pressure can be highly concentrated in each shear band. Such a phenomenon can be the cause of the localizations of soil liquefactions.

It is well known that there are four different types of earthquakes and most of the mass destruction caused by an earthquake over the history is due to tectonic earthquakes (Hubpages, 2011).

The localizations of soil liquefactions can only take place in tectonic earthquakes because they are the only earthquakes with shear bandings resulted from localizations of deformations.

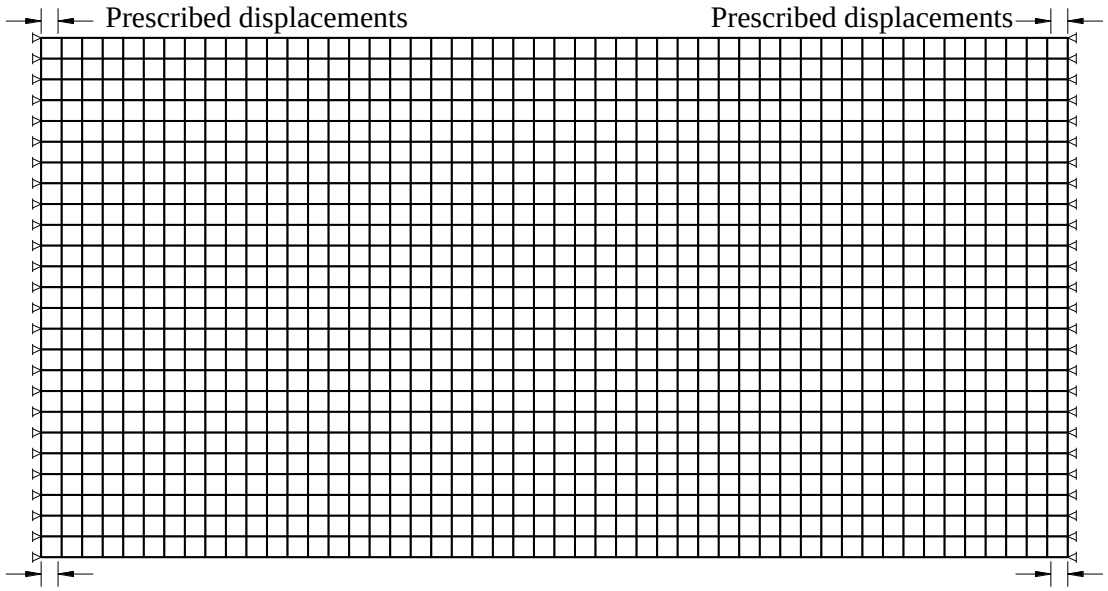

Figure 3. Finite element mesh, boundary conditions and prescribed lateral displacements

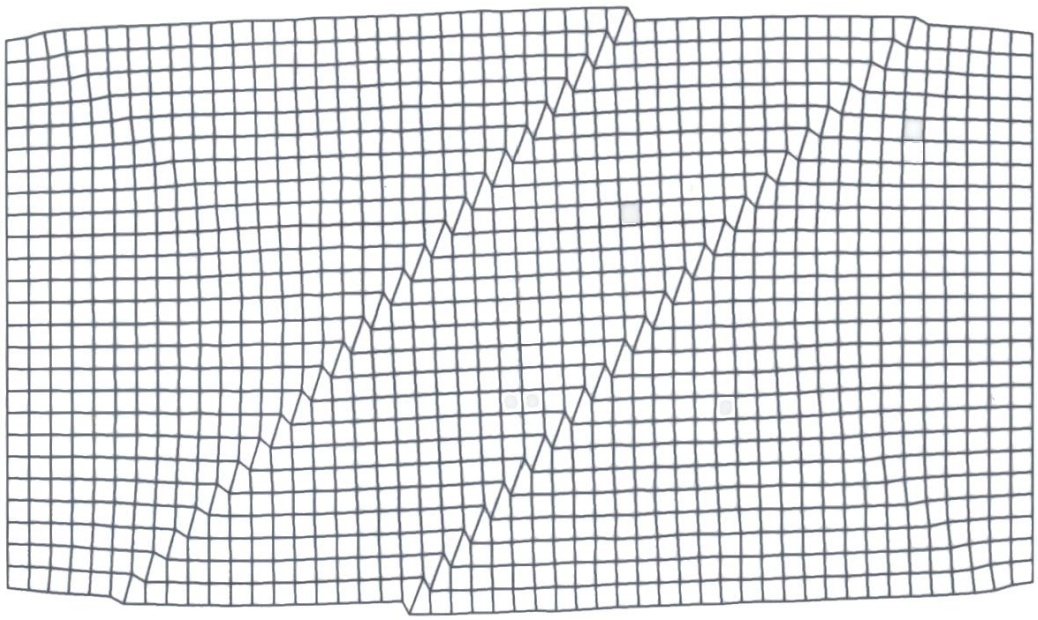

Figure 4. Deformed finite element mesh

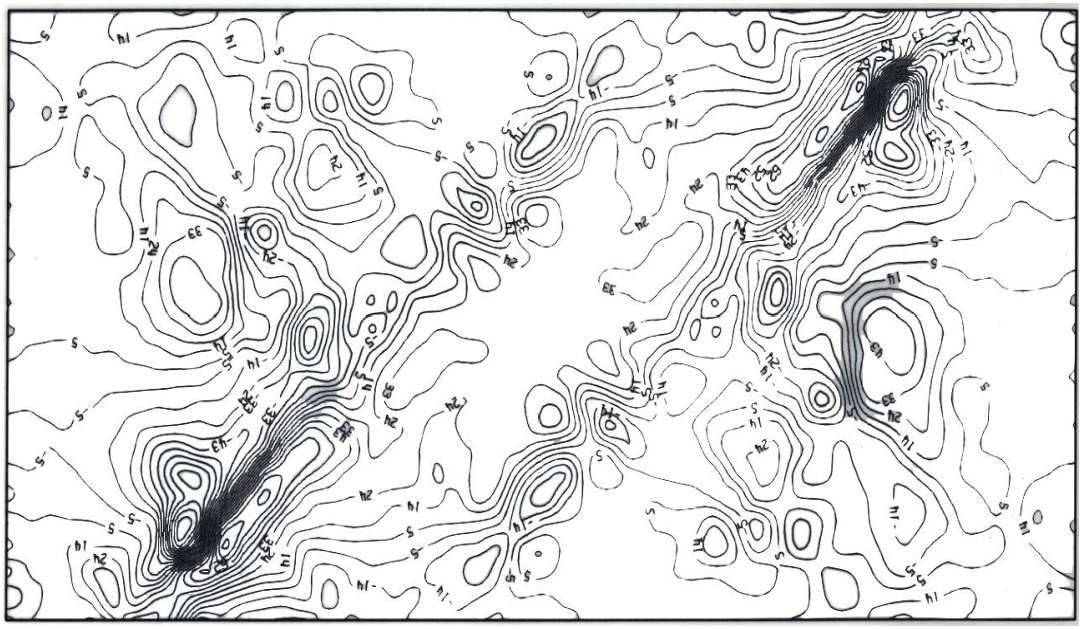

Figure 5. Contours of excess pore water pressures

Even though the conditions before the force is applied to the soil are uniform, homogeneous, and isotropic, once the shear strain of the plate gets deep into plastic range under lateral compression during a tectonic earthquake, localizations of deformations will take place in the

plate due to the loss of ellipticity (Drucker, 1950; Hill, 1962; Mandel, 1966; Rudnicki and Rice, 1975; Rice, 1976; Valanis, 1989), thus leading to highly concentrated excess pore water pressure in shear bands. The brittle fractures of the soils in shear bands have led to greatly increased pore space thus forming the channel for upward ground water flow with sediment entrainment.

Even though the vibration during earthquake will induce excess pore water pressure, there is neither highly concentrated excessive pore water pressure nor channel for upward ground water flow with fragment entrainment in the tectonic plate.

Localizations of soil liquefactions can be divided into tubular soil liquefaction (as shown in Figure 6) and striped soil liquefaction (as shown in Figure 7). The tubular soil liquefaction is resulted from the tectonic plate equipped with tubular water channel similar to piping (Terzaghi and Peck, 1967). Hsu and Chiu (2016) believed that this tubular water channel is formed by intersection of shear textures of different strikes; the striped soil liquefaction is resulted from the tectonic plate equipped with striped water channel, which is the shear band under plane strain conditions (as shown in Figure 4).

As for areas adjacent to soil liquefaction area, even though they are equipped with identical conditions, the localizations of soil liquefactions do not exist because highly concentrated excess pore water pressure and ground water channel were not induced during the earthquake.

Causes of localizations of soil liquefactions include: (1) high shear resistance of foundation soil has led to strain softening behavior; (2) shear banding has led to tectonic local uplift of the Earth surface; (3) loosening of the shear band soil due to brittle fractures; (4) the expanded pore-space of the shear band soil becomes the channel for upward ground water flow with fragment entrainment; (5) the upward flowing water with fragment entrainment will further loosen the shear band soil.

Figure 6. Tubular soil liquefaction took place during Chi Chi Earthquake
(EOU Education Market, 2014)

Figure 7. Striped soil liquefaction took place during Meinong Earthquake
(Liberty Time Net, 2016)

Comparison among various causes of conventional and localizations of soil liquefactions is as shown in Table 1. It appears that the cause of conventional soil liquefaction is totally different from the cause of localizations of soil liquefactions. Obviously the cause of localizations of soil liquefactions can better meet the requirement of actual soil liquefaction as shown in Figure 6 and Figure 7.

The building damage pattern induced by localizations of soil liquefactions during a tectonic earthquake is as shown in Figure 8. This kind of damage pattern is totally different from the damage pattern described by Hsu and Ho (2016) where the building was collapsed due to punching shear failure or tilted due to local shear failure.

Different damage patterns will require different disaster mitigation

Table 1. Comparison among various causes of conventional soil liquefaction and localizations of soil liquefactions

	Traditional soil liquefactions	Localizations of soil liquefactions
Soil conditions	Loose or perfectly plastic	Dense or strain softening
Type of earth-quake causing soil liquefactions	Not specified	Tectonic earthquake
Inducing factor for the major excess pore wa-ter pressure	All-around vibrations	Localizations of deformations
Change of soil conditions	All soils are changed from loose state to dense state	Only the shear band soil is changed from dense state to loose state
Highly concen-trated excess pore water pres-sure	Not exist	Exist in shear bands
Discharge water path for ground water to flow upward	Not exist	The expanded pore-space in the shear band soil

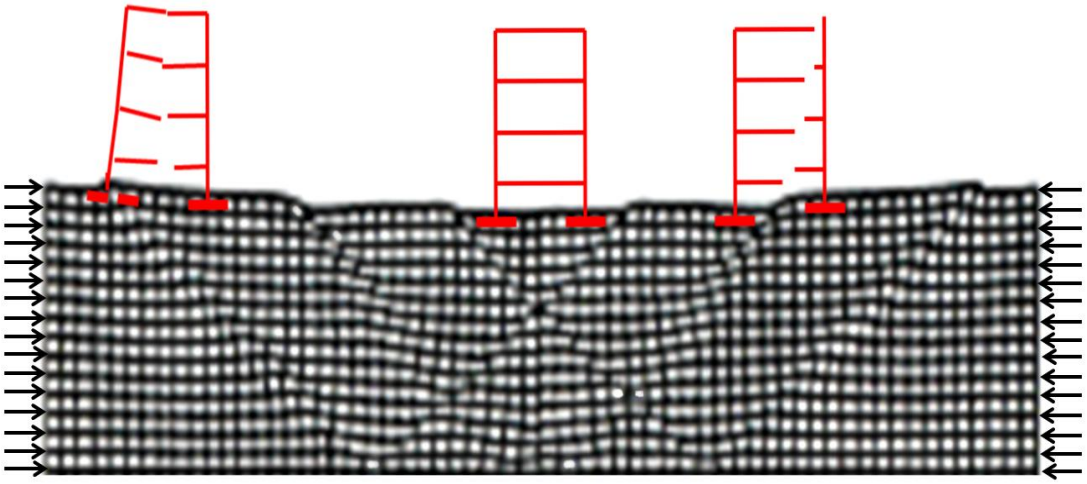

(a) Illustration of building damage pattern

(b) Actual building damage pattern (Pixnet, 2010)

Figure 8. Building damage induced by localizations of soil liquefactions during a tectonic earthquake

(a) The case of misidentifying the punching shear failure of foundation as soil liquefaction (Lee, Der-Ho, 2016)

(b) The case of misidentifying the local shear failure of foundation as soil liquefaction (Moh et al., 2000)

Figure 9. Cases of building damages during earthquake misidentified as to be induced by soil liquefaction

methods related to earthquake, so the building damage induced by foundation punching shear failure (as shown in Figure 9a) or local shear failure (as shown in Figure 9b) must not be misidentified as to be induced by soil liquefaction.

In the past there were soil liquefactions took place in The Lin Family Mansion and Garden in Taichung, Taiwan during the two tectonic earthquakes in 1906 and 1999, respectively. The conventional cause of soil liquefaction fails to explain why soil liquefaction took place at the same location in two consecutive earthquakes. This is because loose sands will be densified after soil liquefaction, and the densified soil will no longer suffer liquefaction

theoretically. However, the aforementioned problem can easily be explained by the cause of localizations of soil liquefactions, because the localizations of soil liquefactions only take place in shear bands with highly concentrated distribution of excess pore water pressure. As long as shear banding takes place at the same location during two consecutive tectonic earthquakes, the soil liquefaction will occur consecutively.

Conclusions And Suggestions

Currently images of soil liquefactions all over the world clearly show that soil liquefactions only take place locally in tectonic earthquakes. For in-depth understanding of the cause of localizations of soil liquefactions during a tectonic earthquake, the authors have carried out simulation and analysis via the program of finite element method compiled based on the elastic-plastic strain softened soil model proposed in this article, and the following six conclusions have been supported by the results and discussion:

1. All-around vibrations can be found in tectonic earthquakes, volcanic earthquakes, collapse earthquakes, and explosion earthquakes. However, localizations of deformations induced shear bandings can only be found in tectonic earthquakes.

2. In the simulation analysis of tectonic earthquakes where a tectonic plate is under lateral compression, when localizations of deformations are captured in a deformed finite element mesh, a highly concentrated excess pore water pressure distribution can be found in each shear band. Such phenomenon is the main cause of localizations of soil liquefactions induced in tectonic earthquakes.

3. Localizations of soil liquefactions include tubular and striped soil liquefactions. Among all localizations of soil liquefactions, the intersection area of shear textures of different strikes and the shear band under plane strain condition will provide water channel for tubular and striped soil liquefactions respectively.

4. The soil liquefaction potential evaluation method currently adopted by Seismic Design Specifications and Commentary of Buildings (2006) is based on conventional cause of soil liquefaction, such that all areas formed by alluvial soils will be evaluated as with liquefaction potentials. Such result of evaluation is totally inconsistent with

the actual situation of soil liquefaction.

5. The conventional cause of soil liquefaction cannot explain the occurrence of soil liquefactions at the same location in two consecutive earthquakes; however, this can be explained by the cause based on localizations of soil liquefactions.

6. Based on conventional cause of soil liquefaction, building damage induced by either punching shear failure or local shear failure of a foundation during an earthquake can be easily misidentified as to be caused by soil liquefaction.

Based on these six aforementioned conclusions, first of all it is strongly recommended in the future study that soil liquefaction potential evaluation should be conducted by adopting the cause of localizations of soil liquefactions such that the announced areas with soil liquefaction potentials can be consistent with the localized areas of actual soil liquefactions; secondly, various causes of building damages during an earthquake should be clearly distinguished such that different building disaster mitigation methods can be proposed in accordance with different causes of damages to achieve the effective disaster mitigation.

Acknowledgements

The support of Institute of Nuclear Energy Research, Atomic Energy Council, Executive Yuan under Project No. INER-NL1030107 is gratefully appreciated.

References

Central Geological Survey, MOEA, "Soil Liquefaction Potential System,"Website:http://www.geologycloud.tw/map/liquefaction/zh-tw, 2016.

Drucker, D. C., "Some implications of work hardening and ideal plasticity," *Quarterly of Applied Mathematics*, Vol. 7, No. 4, pp. 411-418, 1950.

EOU Education Market, "Soil Liquefaction happened at Tatu Creek, Shengang Village, Changhua County, Taiwan, during921 Earthquake ,"website: https://market.cloud.edu.tw/content/primary/country/tc_ua/a004/htm/p3-3.htm, 2014.

Hill, R., "Acceleration waves in solids," *Journal of the Mechanics and Physics of Solids*, Vol. 10, pp. 1-6, 1962.

Hsu, T.-S. and Chiu, S.-E., "Piping Failure Induced by Shear Bandings: Take the Renyitan Reservoir Spillway as an Example," *The International Journal of Organizational Innovation*, Vol, 9, No. 2, pp. 239-259, 2016.

Hsu, T.-S. and Ho, C.-C., "Shear Banding Induced Seismic Building Tilting Failure and Its Control," *International Journal of Organizational Innovation*, Vol. 9, No. 1, pp. 264-281, 2016.

Hubpages, "Types Of Earthquakes," website: http://hubpages.com/education/Types-Of-Earthquakes, 2011.

Ishihara, K. "Liquefaction and Flow Failure during Earthquake," *Géotechnique*, Vol. 43, pp. 351-415, 1993.

Ishihara, K., "Stability of Natural Deposits During Earthquakes," Proceedings, 11th International Conference on Soil Mechanics and Foundation Engineering, San Francisco, Vol. 1, pp. 321-376, 1985.

Iwasaki, T., Tokida, K., and Tatsuoka, F., "Soil Liquefaction Potential Evaluation with Use of the Simplified Procedure," *Proceedings*, First International Conference on Recent Advances in Geotechnical Earthquake Engineering and Soil Dynamics, St. Louis, Missouri, Session 2, Paper 12, 1981.

Japan Road Association, 1996, Guidelines and Comments to Design of Roads and Bridges, Volume V: Earthquake Design (in Japanese).

Kramer, S. L., Geotechnical Earthquake Engineering, *Prentice-Hall*, pp. 366-367, 1996.

Lee, Der-Ho, "Characteristic Investigation of the Geotechnical Environment for Tainan Seismic Disaster Area," Special Conference of 0206 Meinong Earthquake , Department of Civil Engineering, National Cheng-Kung University, 2016.

Liberty Time Net, "The Phenomena of Shear Bandings and Soil Liquefactions in Nanbao Golf Course during 0206Meinong Earthquake," Website:http://news.ltn.com.tw/news/life/breakingnews/1597276, 2016.

Mandel, J., "Conditions de Stabilite et Postulat de Drucker," In *Rheologie et Mechanique des Sols* (Edited by J. Kravtchenko and P. M. Sirieys), Springer, 1966.

Moh, Za-Chieh, Hwang, Richard N., Ueng, Tsou-Shin and Lin, Meei-Ling, "1999 Chi Chi Earthquake of Taiwan," Website: http://www.maa.com.tw/common/publications/2000/2000-037.pdf

Molemkamp, F., "Comparison of Frictional Material Models respect to Shear Band Initiation," *Géotechnique*, Vol. 35, No. 2, pp. 127-143, 1985.

Pixnet, "The Tenth Anniversary of 921: After Rain Comes Sunshine," website: http://crazeroost.pixnet.net/blog/post/, 2010.

Rice, J. R., "The Localization of Plastic Deformation," in Theoretical and Applied Mechanics (Proceedings of the 14th International Congress on Theoretical and Applied Mechanics, Delft, 1976, ed. W.T. Koiter), NorthHolland, Amsterdam, Vol. 1, pp. 207-220, 1976.

Rudnicki, J. W. and Rice, J. R., "Conditions for the localization of deformation in pressure-sensitive dilatants materials," *Journal of the Mechanics and Physics of Solids,* Vol. 23, pp. 371-394, 1975.

Seed, H. B., "Design problems in soil liquefaction." *Journal of Geotechnical Engineering, ASCE,* 113(8), 827-845, 1987.

Seed, R. B. and Harder, L. F., Jr., "SPT-based analysis of cyclic pore pressure generation and undrained residual strength." *Proceedings*, Seed Memorial Symposium, J. M. Duncan, ed., BiTech Publishers, Vancouver, B. C., pp. 351-376, 1990.

Seismic Design Specifications and Commentary of Buildings (Taiwan), 2006.

Seed, H. B., Idriss, I. M., "Simplified Procedure for Evaluating Soil Liquefaction Potential," *Journal of the Soil Mechanics and Foundations Division, ASCE*, Vol. 97, pp. 1249-1273, 1971.

Terzaghi, K., and Peck, R. B., *Soil Mechanics in Engineering Practice*, Second Edition: John Wiley & Sons, New York, pp. 169-170, 1967.

Tokimatsu K., Yoshimi, Y., "Empirical Correlationship of Soil Liquefaction based on NSPT Value and Fine Content," *Soil Foundation*, Vol. 23, pp. 56-74, 1983.

Valanis, K. C., "Banding and stability in plastic materials," *Acta Mech.* Vol. 79, pp. 113-141, 1989.